Etching of Si(100)-2×1 with chlorine: Reaction pathways, energy anisotropies, and atomic-scale phenomena

M. Chander, D. A. Goetsch, C. M. Aldao,* and J. H. Weaver
Department of Materials Science and Chemical Engineering, University of Minnesota, Minneapolis, Minnesota 55455
(Received 8 February 1995)

Rate constants for growth of Cl-induced etch pits on Si(100)-2×1 have been evaluated using data obtained with scanning tunneling microscopy. Etch pits are produced via the removal of a single dimer from a terrace and they grow by removal of adjacent dimers. Two growth modes have been identified, namely, linear growth, where dimer removal occurs along the dimer row direction, and branch formation, where a dimer is removed from an adjacent row. Analysis of the lengths of linear etch pits shows that they follow the most probable Flory-Schulz size distribution. We deduce that the rate constant for linear growth is 4.7±1 times that for branch creation because the energy barrier for dimer removal along the dimer row direction is 0.11±0.02 eV less than that for branch formation. Once a branch is created, its rate constant for linear growth is 2.2±0.5 times greater than along the parent pit since no net step addition is involved. The energy difference for these two types of growth involving a branched pit is 0.06±0.02 eV.

INTRODUCTION

Si(100) etching is of considerable importance to the electronic device industry.[1] The types of etch products and overall etch rates at various temperatures have been established for spontaneous etching with simple halogens.[1–4] Recently, scanning tunneling microscopy (STM) has been used to provide insight into atomic level structural changes that accompany etching.[5–9] Those studies of high-temperature etching of Si(100)-2×1 with Br have shown step retreat via etching along the dimer row.[5] At sufficiently high temperature, etch pits that were one layer deep and were bounded by S_A- and S_B-like steps were formed on the terraces and step etching continued. Since reaction pathways involve atomic level interactions, we postulated[9] that it might be possible to use the data obtained with STM to extract information about etching dynamics and correlate it with the dynamics of surface structure. At the same time, for modeling of these pathways with incorporation of details of surface geometry it was possible that etching phenomena would be too complicated for simple analysis, or the involved energies of the different processes would be too similar, giving rise to random pit distributions.

The STM results for Cl-Si(100) indicate that etch pit initiation involves removal of a dimer from a terrace. Chlorine atoms attack dimers adjacent to this initiation site and the pit grows. Two possibilities exist for such growth, namely, linear growth with dimer removal along the row direction and branch formation with dimer removal from an adjacent row. Since pits grow by stepwise addition of dimer vacancies, this process can be considered along the lines of a polymerization process that involves monomer addition to give linear and branched chains.[10]

Analysis shows that the number density of linear pits follows a Flory-Schulz distribution[11] during the initial stages of etching. The probability of growth is characterized by fitting parameters that provide insight into the rate constants for linear growth and branch formation. Here, we present a kinetic model that relates the rate constants of etch pit growth to energies of formation of steps that are created. Consideration of such a model was encouraged by the Polanyi relation that stipulates that differences in activation energies are related to enthalpy differences for similar processes involving like materials.[12] For dimer removal, the processes are similar, but the enthalpies differ because two types of steps are produced by linear or branch growth. Indeed, analysis that takes into account the number density of pits reveals that the desorption energies along the dimer row and perpendicular to it are different by 0.11±0.02 eV at 850 K, favoring dimer row etching. This is very near the enthalpy difference for the steps so created. With these differences in activation energies, it is possible to predict surface etch pit distributions.

EXPERIMENT

The STM experiments were conducted using a Park Scientific microscope in a chamber with a base pressure of 4×10^{-11} Torr. We used Si(100) wafers oriented within 0.2° of (100). The wafers were rinsed in ethanol prior to introduction into the experimental chamber. They were degassed overnight at 600 °C and flash heated to 1200 °C. The pressure was below 8×10^{-10} Torr during flashing. This procedure resulted in ordered Si(100)-2×1 with defect densities of 2–3 % with characteristic S_A and S_B steps.[13,14] An electrochemical cell was used to provide Cl_2 at a constant flux, with the current through the cell serving as a direct measure of Cl_2 release. Under our experimental conditions, a fluence from the source of ~2 mA s produced a monolayer of Cl on Si(100) at 300 K where 1 ML=6.98×10^{14} atoms cm^{-2}. In all cases, the sample temperature was maintained at 850 K during etching. The samples were

cooled rapidly to room temperature immediately after shutting off the Cl_2 source. STM imaging was done in the constant current mode, as discussed in detail elsewhere.[7]

RESULTS AND DISCUSSION

In Ref. 9, we showed high-resolution STM images of Si(100)-2×1 obtained after exposure to 9.6 mA s Cl_2 at 850 K. The 2×1 nature of the substrate was evident from dimer rows that are oriented along the diagonal.[15] Chlorine adsorbed dissociatively to produce atoms bonded to dimer dangling bonds. While the Cl-bonded dimers were stable at 300 K, volatile $SiCl_2$ could be formed at 850 K.[2,3] Since Si atoms were bound less tightly at steps than on terraces, it was easier to remove atoms from the step edges. At the same time, material removal also occurred from the terraces. Once initiated, growth was propagated by dimer removal along and perpendicular to the dimer row direction to produce etch pits, *P*, that were one atom layer deep. As a consequence of dimer breaking to produce $SiCl_2$, some Si atoms were ejected onto the surface where they could form regrowth islands, *I*, that are one layer high.

In this paper, we focus on the growth of terrace etch pits. Such etch pits can be characterized as linear pits, *L*, that are one row wide; linear pits that have a dimer vacancy branch on an adjacent row, $L+B$; pits that are two rows wide, $L+L$; and so on. They can be characterized further according to the location of the branch site. The smallest pits are single dimer vacancies. The fact that the number density of these pits is much larger than the pit density of intrinsic dimer vacancies on the surface implies that intrinsic defects play a relatively minor role in pit initiation.

Two distinct mechanisms can be postulated for lateral pit growth. One involves expansion outward from a dimer vacancy. The other involves creation of independent dimer vacancies, followed by thermally activated migration and vacancy coalescence. Such migration has been observed for isolated vacancies produced by ion bombardment of Si(100)-2×1 at ~723 K.[16] To assess it here, we annealed etched surfaces at 850 K. While continued etching consumed residual surface Cl, analysis showed no significant change in the number densities of pits of various sizes. Reduced vacancy diffusion relative to clean Si(100) can be attributed to the presence of Cl, as for Br-Si(100).[8] This is a significant factor, since the halogen atoms accumulate during dosing. From analysis of the STM images, Chander *et al.*[9] deduced that the surfaces that they studied after exposure at 850 K were approximately 30% covered with Cl.[17] The analysis here is for the same surfaces. We conclude that vacancy coalescence does not account for the observed morphology, and we focus on dimer removal from sites next to an existing pit.[18]

Terrace pitting is initiated via formation of a single dimer vacancy, *V*. Growth along the dimer row direction produces a double vacancy, *VV*. This unit can continue with linear growth to *VVV* or it can branch by removal of a dimer from an adjacent row. The branched pit can be consumed via linear growth of the major chain, linear

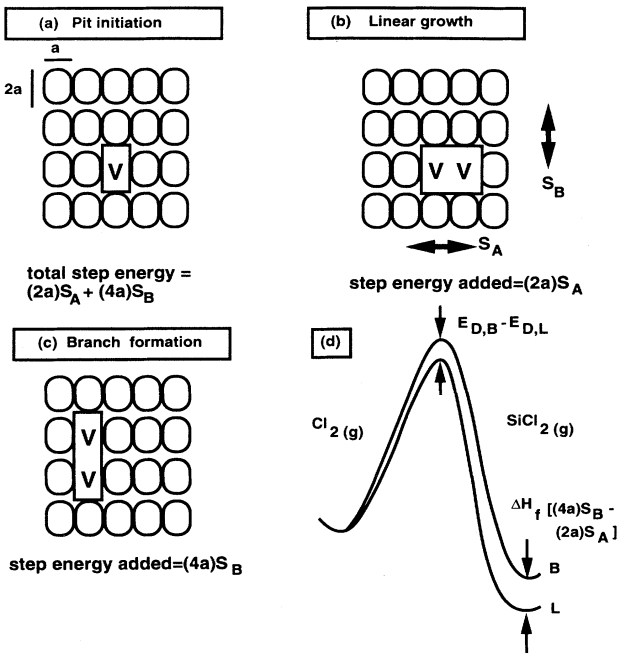

FIG. 1. A schematic of pit growth in terms of the enthalpies associated with creation of steps of S_A and S_B type. (a) corresponds to creation of a single vacancy on a terrace, (b) reflects linear growth of this vacancy along the dimer row direction, and (c) depicts branch creation from a single vacancy. The bold arrows S_A and S_B are parallel to the step edges. The sketch in (d) represents the enthalpies involved in etching going from the state depicted in (a) to (b) or (c) with the process that can be written $V+Cl_2 \xrightarrow{L} VV+SiCl_2(g)$ and $V+Cl_2 \xrightarrow{B} \underset{V}{V}+SiCl_2(g)$. The energy barriers associated with etching along the dimer row direction and branch formation are $E_{D,L}$ and $E_{D,B}$. The difference in these barriers is determined to be 0.11±0.02 eV.

growth from the branch, or further branching, as shown in Ref. 9. Subsequent growth can be explained via such a net, but the number of channels increases. The population distribution on the surface reflects the rates at which new species are generated and consumed.

The enthalpy of formation of a pit can be estimated by recognizing that a pit creates "miniature" step edges. Removal of a single dimer from a terrace creates a high-energy S_B step of length $4a$ perpendicular to the dimer row direction and a low-energy S_A step of length $2a$ along the dimer row direction, where a is the unit-cell dimension, 3.84 Å. This is shown schematically in Fig. 1(a). In linear growth, dimers are removed along the row direction, Fig. 1(b), adding $2a$ step length of an S_A edge for each dimer and none of S_B. In branch formation, removal from adjacent rows involves addition of $4a$ of S_B edge and none of S_A, Fig. 1(c). Branch formation exposes the second row to linear growth, expanding the width of the pit.

Figure 1(d) depicts the enthalpies of formation and the energy barriers for dimer removal for the two pathways. Both processes are exothermic in the presence of Cl_2,

with the release of $SiCl_2$ (gas). Both processes also require less energy than removal of an isolated dimer from the terrace. The enthalpies of formation reflect the overall lengths of the S_A and S_B edges with linear growth to state L favored over branch formation to state B. For clean Si(100) 2×1, the energy difference is $E(S_B)-E(S_A)=0.14$ eV per unit length (Ref. 19). Pit anisotropy is dictated by the energy difference $E_{D,B}-E_{D,L}$. The analysis of etch patterns makes it possible to determine this energy difference. Note that the sketch of Fig. 1(d) is consistent with the Polanyi relation, because the barrier leading to the more favorable thermodynamic state is smaller than that for the less favorable state.

Linear growth

According to the etching scheme of Fig. 1, linear pits, L, will be produced by the addition of dimer vacancies along the row direction. Formation of a single branch will produce an $L+B$ structure, which can elongate to an $L+L$ structure or branch further. Competition between linear growth and branch creation accounts for the pit size and shape distribution. This is similar to polymer chain growth because both involve the addition of entities to reach the final product.

Associated with linear growth is a probability, p_L, that describes linear growth, with $(1-p_L)$ accounting for branch formation. p_L should decrease with pit length as more sites along the pit become available for branch formation. While analysis of the STM images shows that this is the case, branching occurs preferentially at the ends so that p_L is not greatly affected. Under conditions where p_L remains constant, the chain size distribution follows the most probable or Flory-Schulz distribution.[10,11] The areal density of chains with i units is then $[V_i]=p_L^{i-1}[V]$, where P_L^{i-1} accounts for $i-1$ growth events with probability p_L starting from the unit with size 1. A plot of $\ln([V_i]/[V])$ vs $(i-1)$ gives a straight line with slope $\ln(p_L)$. While it is reasonable to expect that linear growth of pits will follow this most probable distribution, there are complications that would randomize the distribution, such as limited availability of Cl and interaction between pits. The test, then, lies in analysis of the STM results.

Vacancy creation at the end of a pit involves three steps. First, an adsorbed Cl atom in a state SiCl diffuses to a Si atom adjacent to pit V_i of size i to form an activated pit V_i^*, as depicted in Fig. 2. The rate constant of this propagation step is $k'_{p,L}$. The second step involves diffusion of another Cl atom to V_i^* to produce V_i^{**} (propagation rate constant $k''_{p,L}$). This represents two Cl atoms bound to a Si atom having two back bonds in a transition state. Desorption of a $SiCl_2$ molecule leads to pit growth to V_{i+1} (desorption rate constant k_D). Alternatively, the Cl atoms can detach from active pits V_i^* and V_i^{**} with termination rate constants $k'_{t,L}$ and $k''_{t,L}$. We assume that bonding to a site V_i^* is favored over terrace bonding so that there is a bias toward V_i^* population. V_i^{**} is a short-lived state[20] that is produced and lost a large number of times before desorption occurs. In an analogous fashion, Cl adsorption on dimers adjacent to the linear pit produces a branch via intermediates that we denote V^* and V^{**}.

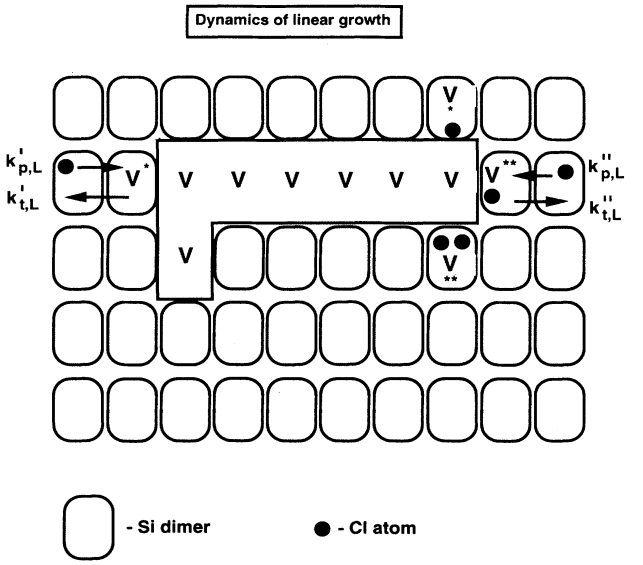

FIG. 2. Representation of the dynamic processes involved in dimer removal for a pit of arbitrary shape and length. k's represent the propagation and termination rate constants for processes that lead to or away from activation of dimers at pit ends or branch sites, subscripted L and B, respectively. V^* denotes a dimer with a single Cl atom and V^{**} denotes a dimer with two Cl atoms on a single Si atom at the end of the pit.

The etching part of this scheme explicitly accounts for the removal of a single atom of the dimer. Pit growth, however, requires the removal of both atoms, since single atom vacancies are not observed. The second atom can be etched in a fashion similar to the first or it can be ejected onto the surface to contribute to terrace regrowth or be etched.[5] The various ways of second atom removal cannot be distinguished and the rate constant for pit growth, k_D, must be considered as an overall rate constant for dimer removal processes.

In the following, we consider the generation and consumption steps for a double-vacancy pit, using subscripts 1, 2 to refer to pit sizes. The rate constants for propagation, termination, and desorption, are subscripted L for linear growth and B for the branch growth. The scheme remains the same irrespective of linear or branched growth.

Generation of a double vacancy pit from the linear growth of a single dimer vacancy follows from

$$V+\mathrm{SiCl}\underset{k'_{t,L,1}}{\overset{k'_{p,L,1}}{\rightleftharpoons}}V^*+\mathrm{Si}\,, \tag{1}$$

$$V^*+\mathrm{SiCl}\underset{k''_{t,L,1}}{\overset{k''_{p,L,1}}{\rightleftharpoons}}V^{**}+\mathrm{Si}\,, \tag{2}$$

$$V^{**} \xrightarrow{k_{D,L,1}} VV + \mathrm{SiCl}_{2(g)} . \quad (3)$$

Consumption of VV by growth into VVV follows from

$$VV + \mathrm{SiCl} \underset{k'_{t,L,2}}{\overset{k'_{p,L,2}}{\rightleftharpoons}} VV^{*} + \mathrm{Si} , \quad (4)$$

$$VV^{*} + \mathrm{SiCl} \underset{k''_{t,L,2}}{\overset{k''_{p,L,2}}{\rightleftharpoons}} VV^{**} + \mathrm{Si} , \quad (5)$$

$$VV^{**} \xrightarrow{k_{D,L,2}} VVV + \mathrm{SiCl}_{2(g)} . \quad (6)$$

Consumption of VV by branching into $\underset{V}{V}V$ follows from

$$VV + \mathrm{SiCl} \underset{k'_{t,B,2}}{\overset{k'_{p,B,2}}{\rightleftharpoons}} \underset{*}{V}V + \mathrm{Si} , \quad (7)$$

$$\underset{*}{V}V + \mathrm{SiCl} \underset{k''_{t,B,2}}{\overset{k''_{p,B,2}}{\rightleftharpoons}} \underset{**}{V}V + \mathrm{Si} , \quad (8)$$

$$\underset{**}{V}V \xrightarrow{k_{D,B,2}} \underset{V}{V}V + \mathrm{SiCl}_{2(g)} . \quad (9)$$

The areal density of VV pits is $[VV]$. The net rate of change of $[VV]$ follows from Eqs. (3), (4), and (7), where the rate is the product of its rate constant times the areal density of the reactants. In general, the goal is to relate the areal density of final product to that of its predecessor, in this case $[VV]$ to $[V]$. This can be done by writing

$$\begin{aligned}\frac{d[VV]}{dt} = {} & k_{D,L,1}[V^{**}] - k'_{p,L,2}[VV][\mathrm{SiCl}] \\ & + k'_{t,L,2}[VV^{*}][\mathrm{Si}] - k'_{p,B,2}[VV][\mathrm{SiCl}] \\ & + k'_{t,B,2}[\underset{*}{V}V][\mathrm{Si}] . \end{aligned} \quad (10)$$

Equation (10) can be simplified by assuming that the areal distributions for the different sized pits do not change in time, an assumption that is confirmed by experimental verification of the sizes studied. This implies that

$$\begin{aligned}\frac{d[V^{**}]}{dt} = {} & k''_{p,L,1}[V^{*}][\mathrm{SiCl}] - k''_{t,L,1}[V^{**}][\mathrm{Si}] \\ & - k_{D,L,1}[V^{**}] = 0 . \end{aligned} \quad (11)$$

Accordingly, we can write

$$[V^{**}] = \frac{k''_{p,L,1}[V^{*}][\mathrm{SiCl}]}{k''_{t,L,1}[\mathrm{Si}] + k_{D,L,1}} . \quad (12)$$

Likewise,

$$\frac{d[V^{*}]}{dt} = 0$$

so that

$$[V^{*}] = \frac{k'_{p,L,1}[V][\mathrm{SiCl}] + k''_{t,L,1}[V^{**}][\mathrm{Si}]}{k'_{t,L,1}[\mathrm{Si}] + k''_{p,L,1}[\mathrm{SiCl}]} . \quad (13)$$

Combining the expressions for $[V^{**}]$ and $[V^{*}]$ gives $[V^{**}] = X_{L,1}[V]$, where

$$X = \frac{k'_{p}k''_{p}[\mathrm{SiCl}]^2}{k_{D}k'_{t}[\mathrm{Si}] + k_{D}k''_{p}[\mathrm{SiCl}] + k'_{t}k''_{t}[\mathrm{Si}]^2} , \quad (14)$$

with proper subscripts. Physically, X relates the areal density of $[V^{**}]$ to $[V]$ so that the number of activated sites is proportional to the number of vacancies. $[VV^{*}]$ and $[\underset{*}{V}V]$ can also be evaluated from $d[VV^{*}]/dt = 0$ and $d[\underset{*}{V}V]/dt = 0$, for substitution in Eq. (10), and the expressions are

$$[VV^{*}] = \frac{k'_{p,L,2}[VV][\mathrm{SiCl}] + k''_{t,L,2}[VV^{**}][\mathrm{Si}]}{k'_{t,L,2}[\mathrm{Si}] + k''_{p,L,2}[\mathrm{SiCl}]} , \quad (15)$$

and

$$[\underset{*}{V}V] = \frac{k'_{p,B,2}[VV][\mathrm{SiCl}] + k''_{t,B,2}[VV^{**}][\mathrm{Si}]}{k'_{t,B,2}[\mathrm{Si}] + k''_{p,B,2}[\mathrm{SiCl}]} . \quad (16)$$

Substituting $[V^{**}]$, $[VV^{*}]$, and $[\underset{*}{V}V]$ in Eq. (10) and rearranging terms gives

$$\begin{aligned}\frac{d[VV]}{dt} = {} & k_{D,L,1}X_{L,1}[V] - k_{D,L,2}X_{L,2}[VV] \\ & - k_{D,B,2}X_{B,2}[VV] . \end{aligned} \quad (17)$$

Assuming steady-state conditions for VV pit density so that $d[VV]/dt = 0$ gives

$$[VV] = \frac{k_{D,L,1}X_{L,1}}{k_{D,L,2}X_{L,2} + k_{D,B,2}X_{B,2}}[V] . \quad (18)$$

This relates the areal density of double vacancies to that of single vacancies under conditions of growth determined by the rate constants and the concentrations [Si] and [SiCl].

The propagation and termination rate constants that reflect diffusion of Cl to and from a given pit will depend on geometric details around the pit and the energetics of each bonding site. Such details are not accessible to our measurements and, in any case, the Cl concentration is large and diffusion at 850 K is facile.[17] Instead, we obtain information about the distribution of pits by counting a large number of them. We have obtained pit densities over an area of $\sim 0.15 \times 0.15\ \mu\mathrm{m}^2$, with the total number of pits being ~ 1500–2000 for each of the conditions of Cl flux and fluence. We found no noticeable change in the p_L values by including more pits. While $SiCl_2$ desorption rate constants will depend on the transition states formed at the ends of pits, they should be largely independent of pit length.

Deleting the subscripts 1,2 for the sizes gives the relationship between pit size i and $i-1$, namely, $[V_i] = p_L[V_{i-1}]$ with $[V_{i-1}] = p_L[V_{i-2}]$, . . . and $[V_2] = p_L[V]$. Hence, $[V_i] = p_L^{i-1}[V]$, where

$$p_L = \frac{k_{D,L}X_L}{k_{D,L}X_L + k_{D,B}X_B} . \quad (19)$$

This is the expression for the most probable distribution, such that p_L is the ratio of the rate of production to the

sum of rates of production and disappearance of a given pit size.

Reference 9 showed $\ln([V_i]/[V])$ vs $i-1$ for linear pits on Si(100)-2×1 after etching at 850 K. Linear regression showed that most points fit the straight line for a variety of flux and fluence conditions. The slopes under a 95% confidence interval give p_L's of 0.68±0.05, 0.69±0.03, and 0.71±0.05, respectively.[9,21] The constancy of p_L under various conditions of flux and fluence indicates etching under quasi-steady-state conditions, where [SiCl] and [Si] do not affect the value of parameter X and, hence, p_L. This implies that all growth sites have sufficient Cl irrespective of etching parameters and there is no strong pit-pit interaction.

In the above analysis, we have assumed quasi-steady-state conditions such that the generation and consumption of pits of any size was equilibrated. In fact, this is a very good approximation for all pit sizes studied, except the single vacancies. As the portion of the surface covered by pits becomes an appreciable fraction of the total surface, arriving Cl atoms attacking the existing pits, the generation of single vacancies decreases, and our simple picture is no longer valid. The low values for $[V]$ relative to $[VV]$ and larger pits evident in Fig. 3 of Ref. 9 can be attributed to this consideration.

Energy barrier differences for linear growth and branch formation

The fact that p_L is a constant for linear pit growth makes it possible to determine the energy barrier differences for linear growth and branch formation. First, we note that $K_D/k_t \ll 1$ for both linear and branch growth, because the activation energy of $SiCl_2$ desorption is at least 1 eV higher than the activation energy for Cl surface diffusion.[22] Accordingly, X can be simplified to

$$X=\frac{(k_p'/k_t')(k_p''/k_t'')[\mathrm{SiCl}]^2}{[\mathrm{Si}]^2} .$$

Second, Cl diffusion to and from pits to change the concentration of active sites is not expected to be significantly different for linear and branch growth. In any case, the Cl concentration is high enough that diffusion is not a rate limiting process.[17] Hence, the parameters $(k_p/k_t)_L'/(k_p/k_t)_B'$ and $(k_p/k_t)_L''/(k_p/k_t)_B''$ are nearly unity and X_L/X_B is approximately one. The probability of linear growth is then simply

$$p_L=\frac{1}{1+\dfrac{k_{D,B}}{k_{D,L}}} . \tag{20}$$

Since there are two sites for linear growth per pit, a statistical factor of two is inherent in $k_{D,L}$. Similarly, there are two possible sites for branching at every vacancy. While one would expect that the statistical factor for branching would be $2\times i$, our observations show that branching at end points is dominant. This might be due to a lower corner energy involved in producing a branch at the end as compared to the middle. In any case, the statistical factor for branching is only four (a factor of two from each end), so that

$$p_L=\frac{1}{1+\dfrac{4k_{D,B}}{2k_{D,L}}} . \tag{21}$$

Since p_L was deduced above to be 0.7±0.05, this gives $k_{D,B}/k_{D,L}=0.21\pm0.05$.

Finally, general rate constants can be written $K=\sigma^*\exp(-E/kT)$. The prefactors for desorption for linear and branch growth are governed by the entropies of the transition states. In turn, these entropies depend on the lengths and energies of the various bonds in the transition states. Since these differences are small, the prefactors cannot account for the difference in the two rate constants and we set them equal. Accordingly, $k_{D,B}/k_{D,L}=\exp[-(E_{D,B}-E_{D,L})/kT]=0.21\pm0.05$. The difference in activation energies is then $E_{D,B}-E_{D,L}=0.11\pm0.02$ eV.

The desorption of a $SiCl_2$ unit from either a branch site or a linear site will involve breaking two Si-Si backbonds and a dimer bond. Since step formation is the result of the breaking of these bonds, the difference in the formation energies of the steps should be reflected in the barriers involved in bond breaking. Indeed, there is often a relationship between activation barriers and enthalpies of formation for a family of reactions of the sort described here by the semiempirical Polanyi relationship.[12] Calculations[9] for clean Si(100)-2×1 predict a formation energy difference of $E(S_B)-E(S_A)=0.14$ eV. Our results for the activation barriers indicate that $E_{D,B}-E_{D,L}=0.11\pm0.02$ eV. Accordingly, we have both quantities of interest, the difference in energy barriers and enthalpies.

Calculations for Si(100)-2×1 indicate differences in energies for nonbonded S_B' and rebonded S_B step edges.[9] Since the energy per atom on the edge is greater for an S_B' step than an S_B step, one would expect to see different ratios of $k_{D,B}/k_{D,L}$ for even- and odd-sized pits. We find no differences in the experimental values for even- and

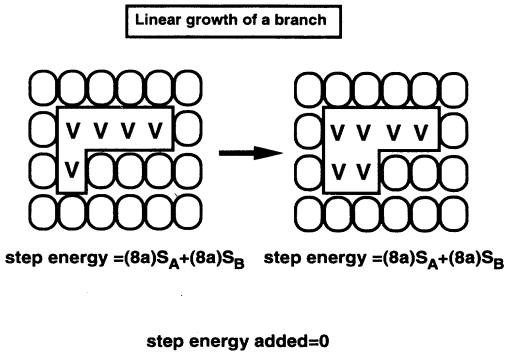

FIG. 3. Schematic showing that linear growth of a branch adjacent to a parent row does not involve step creation. In contrast, linear growth of the parent does involve a change in enthalpy for the system. The activation energies for these two processes reflect these thermodynamic states and differ by 0.06±0.02 eV.

odd-sized pits. This indicates that Cl affects the bonding character at the S_B and S_B' edges, so that differences in energy barriers and formation energies are no longer pronounced.

Linear growth from a branch

Step energy considerations suggest that linear growth of a branch adjacent to the parent L pit should be energetically more favorable than the growth of the pit, since no net step creation is involved. This is depicted in Fig. 3. To investigate the kinetics of such growth, we have analyzed linear pits that have just one branch at the end. Such $[{}^{V_{i-1}}_{V}]$ pits can be produced via branch creation on V_{i-1} and via linear growth of the parent row. Now the statistical factors involved in the generation of $L+B$ pits of size greater than 3 (2 linear + 1 branch) are 4 for $k_{D,B}$ for the first pathway and 1 for $k_{D,L}$ for the second pathway. In principle, growth of the linear unit can also occur at the branched end, but such units with a branch that is not at the end are not counted here. Inclusion of such a pathway complicates the mathematical description below. In any case, these pits can be consumed by linear growth, branch creation, and linear growth of the branch. The statistical factors for the three pathways are 3 for $k_{D,L}$ (2 from the two ends of the parent row and 1 from growth of the branch opposite to the parent row), 4 for $k_{D,B}$ (as before), and 1 for $k_{D,LB}$ that denotes the growth of the branch adjacent to the parent row. The steady-state areal density for $L+B$ units for i greater than 3 can be expressed as

$$\begin{bmatrix} V_{i-1} \\ V \end{bmatrix} = \frac{4k_{D,B}X_B[V_{i-1}]}{3k_{D,L}X_L+4k_{D,B}X_B+k_{D,LB}X_{LB}} + \frac{k_{D,L}X_L\begin{bmatrix} V_{i-2} \\ V \end{bmatrix}}{3k_{D,L}X_L+4k_{D,B}X_B+k_{D,LB}X_{LB}} . \quad (22)$$

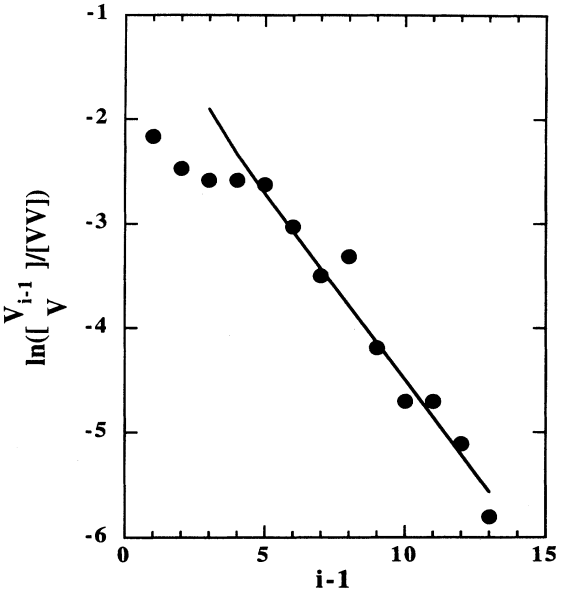

FIG. 4. A plot of $\ln[{}^{V_{i-1}}_{V}]/[VV]$ vs $(i-1)$, where the circles represent experimental data and the line was obtained from Eq. (23). From the fit to the data, we deduce that $k_{D,LB}/k_{D,L}=2.2\pm0.5$, such that the probability of linear growth from the branched unit is twice that of linear growth from the parent chain for i greater than 3. For shorter units, statistical factors associated with the number of possible growth and branch sites affect the general behavior depicted by the line.

$[{}^{V_{i-2}}_{V}]$, can again be expressed in terms of $[V_{i-2}]$ and $[{}^{V_{i-3}}_{V}]$. Thus, we can derive an analytical expression that relates $[{}^{V_{i-1}}_{V}]$ to $[VV]$ and $[{}^{VV}_{V}]$. Assuming that all pits have sufficient Cl for growth, $X_L \sim X_B \sim X_{LB}$ and the expression reduces to

$$\begin{bmatrix} V_{i-1} \\ V \end{bmatrix} = \frac{\left[\frac{4k_{D,B}}{k_{D,L}}\right]}{\left[3+\frac{4k_{D,B}}{k_{D,L}}+\frac{k_{D,LB}}{k_{D,L}}\right]}\left[\frac{1}{1+\frac{2k_{D,B}}{k_{D,L}}}\right]^{i-3}\left[1-\left[\frac{\frac{1+2k_{D,B}}{k_{D,L}}}{3+\frac{4k_{D,B}}{k_{D,L}}+\frac{k_{D,LB}}{k_{D,L}}}\right]^{i-2}\Bigg/\left[1-\frac{1+\frac{2k_{D,B}}{k_{D,L}}}{3+\frac{4k_{D,B}}{k_{D,L}}+\frac{k_{D,LB}}{k_{D,L}}}\right][VV]\right] + \left[\frac{1}{3+\frac{4k_{D,B}}{k_{D,L}}+\frac{k_{D,LB}}{k_{D,L}}}\right]^{i-3}\begin{bmatrix} VV \\ V \end{bmatrix} . \quad (23)$$

The ratio $k_{D,LB}/k_{D,L}$ is the only unknown in Eq. (23), $k_{D,B}/k_{D,L}$ being known from the previous analysis. Hence, we can fit the experimental data for $L+B$ pit density using Eq. (23) to obtain $k_{D,LB}/k_{D,L}$. (Again, the branch is constrained to be at the pit end.)

Figure 4 shows $\ln[{}^{V_{i-1}}_{V}]/[VV]$ vs $(i-1)$ obtained from the experimental data using circles. The values calculated using Eq. (23) constitute the line when $k_{D,LB}/k_{D,L}=2.2\pm0.5$. The experimental data points in Fig. 4 represent average numbers deduced from experiments done at different flux and fluence (Ref. 9). Averaging data sets that represent different conditions of Cl flux and fluence is justified by the analysis for L pits that indicated a similar kinetic state for all three sets.

From Fig. 4, it is evident that pits of the form $\underset{V}{V}$ are present in too low areal densities to fall on the straight

line dictated by the model. Their low density can be easily understood as a consequence of the statistical factors involved in their generation and consumption. These pits are generated by the branching of a single vacancy V with a statistical factor of only 2 compared to 4 for longer chains. Moreover, they are consumed through linear growth, which dominates and has four sites available, and branch creation, although less probable than linear growth, and again has a statistical factor of 2. As seen in Fig. 4, the low value of $\frac{V}{V}$ suppresses the concentration of pits that grow from it. However, when $i=5$, these considerations related to small pits are no longer important and growth is dominated by elongation. Mathematically, this corresponds to the diminished importance of the second term of Eq. (23), indicating that most $[\frac{V}{V}^{i-1}]$ units have originated from dimer $[VV]$ chains.

The differences in energy barriers between the pathways of linear growth of the parent row and the linear growth from the branch can again be deduced assuming that the prefactors are approximately the same. Using $k_{D,LB}/k_{D,L}=2.2\pm0.5$, we find $E_{D,L}-E_{D,LB}=0.06\pm0.02$ eV. This shows quantitatively that the pathway indicated by the bold arrow from $\frac{V}{V}V$ in Fig. 1 (linear growth of a branch) has a lower energy barrier than that indicated by the solid arrow (linear growth of the parent row). Again, this kinetic consideration is consistent with the Polanyi relation because the former pathway involves no increase in the step energy, while the latter does. In the spirit of Fig. 1(d), LB growth produces a state of lower energy than L and it has a lower barrier for growth than does L growth.

CONCLUSIONS

This study represents an attempt to estimate the kinetic parameters for structural changes on the atomic scale. We have been able to determine the energies associated with pit growth, quantifying the channels identified in Ref. 9. Moreover, the generality of this approach makes it useful for deriving similar information in other systems. Such knowledge of kinetic parameters can be used for developing a comprehensive kinetic model that would allow the prediction of atomic details of surfaces exposed to various conditions of etchant flux, fluence, and temperature, and hence for the production of nanopatterned surfaces.

ACKNOWLEDGMENTS

This work was supported by Office of Naval Research. The authors thank R. J. Pechman, D. Rioux, and D. W. Owens for technical assistance and discussion.

*Permanent address: Institute of Materials Science and Technology (INTEMA), Universidad Nacional de Mar del Plata–CONICET, Juan B. Justo 4302, 7600 Mar del Plata, Argentina.

[1]H. F. Winters and J. W. Coburn, Surf. Sci. Rep. **14**, 161 (1992).
[2]R. B. Jackman, H. Ebert, and J. S. Foord, Surf. Sci. **176**, 183 (1986).
[3]Q. Gao, C. C. Cheng, P. J. Chen, W. J. Choyke, and J. T. Yates, Jr., J. Chem. Phys. **98**, 8308 (1993).
[4]R. B. Jackman, R. J. Price, and J. S. Foord, Appl. Surf. Sci. **36**, 296 (1989).
[5]M. Chander, Y. Z. Li, J. C. Patrin, and J. H. Weaver, Phys. Rev. B **47**, 13 035 (1993).
[6]M. Chander, Y. Z. Li, D. Rioux, and J. H. Weaver, Phys. Rev. Lett. **71**, 4154 (1993).
[7]D. Rioux, M. Chander, Y. Z. Li, and J. H. Weaver, Phys. Rev. B **49**, 11 071 (1994).
[8]R. Rioux, R. J. Pechman, M. Chander, and J. H. Weaver, Phys. Rev. B **50**, 4430 (1994).
[9]M. Chander, D. A. Goetsch, C. M. Aldao, and J. H. Weaver, Phys. Rev. Lett. **74**, 2014 (1995).
[10]See, for example, *Polymer Synthesis,* edited by P. Rempp and E. W. Merrill (Hüthig and Wepf Verlag, New York, 1986), Chaps. 2 and 3.
[11]P. J. Flory, Chem. Rev. **39**, 137 (1946).
[12]M. Boudart, *Kinetics of Chemical Processes* (Butterworth, Stoneham, MA, 1991).
[13]B. S. Swartzentruber, Y.-W. Mo, M. B. Webb, and M. G. Lagally, J. Vac. Sci. Technol. A **7**, 2901 (1989).
[14]M. Chander, Y. Z. Li, J. C. Patrin, and J. H. Weaver, Phys. Rev. B **48**, 2493 (1993).
[15]See R. J. Hamers, R. M. Tromp, and J. E. Demuth, Phys. Rev. B **34**, 5343 (1986); R. J. Hamers, U. K. Kohler, and J. E. Demuth, J. Vac. Sci. Technol. A **8**, 195 (1990).
[16]P. Bedrossian and T. Klitsner, Phys. Rev. Lett. **68**, 646 (1992).
[17]The value of 30% Cl concentration is based on atomically resolved STM images of etched surfaces. Cl-covered dimers show different contrast and two atomic features per dimer are apparent, unlike clean Si dimers in the occupied states STM images. The effect has been discussed in Ref. 7 for Br-Si(100)-2×1. Vacancy diffusion occurred after complete desorption of Br and Cl at ~1100 K and the surface recovered to that characteristic of the starting surface.
[18]It is possible that only one atom of the dimer is removed initially, the second atom being loosely held in the absence of the dimer bond [Z. Zhang and H. Metiu, Phys. Rev. B **48**, 8166 (1993)]. While the differences in absolute energies from this structure might differ for pairwise removal, the step creation picture should still be valid.
[19]D. J. Chadi, Phys. Rev. Lett. **59**, 1691 (1987).
[20]According to Ref. 3, this short-lived $SiCl_2$ unit is not observed in electron-energy-loss spectra under various conditions of Cl adsorption and etching.
[21]To confirm statistical validity, we analyzed the data sets three times after varying the drift correction to the images. The p values remained the same within the range of the error.
[22]The Si-Cl bond energy is ~4 eV [*CRC Handbook of Chemistry and Physics,* 69th ed. (CRC, Boca Raton, 1989)]. Assuming an activation energy for diffusion of 1 eV gives $\sim 10^7$ hops per second for Cl on Si at 850 K, if all sites are available.